DESY-23-094

Constraining Post-Inflationary Axions with Pulsar Timing Arrays

Géraldine Servant[1, 2, *] and Peera Simakachorn[3, †]

[1]*Deutsches Elektronen-Synchrotron DESY, Notkestr. 85, 22607 Hamburg, Germany*
[2]*II. Institute of Theoretical Physics, Universität Hamburg, 22761, Hamburg, Germany*
[3]*Instituto de Física Corpuscular (IFIC), Consejo Superior de Investigaciones Científicas (CSIC) and Universitat de València, 46980, Valencia, Spain*

(Dated: July 7, 2023)

Models that produce Axion-Like-Particles (ALP) after cosmological inflation due to spontaneous $U(1)$ symmetry breaking also produce cosmic string networks. Those axionic strings lose energy through gravitational wave emission during the whole cosmological history, generating a stochastic background of gravitational waves that spans many decades in frequency. We can therefore constrain the axion decay constant and axion mass from limits on the gravitational wave spectrum and compatibility with dark matter abundance as well as dark radiation. We derive such limits from analyzing the most recent NANOGrav data from Pulsar Timing Arrays (PTA). The limits are compatible with the slightly stronger $N_{\rm eff}$ bounds on dark radiation for ALP masses $m_a \lesssim 10^{-10}$ eV. On the other hand, for heavy ALPs with $m_a \gtrsim 0.1$ GeV and $N_{\rm DW} \neq 1$, new regions of parameter space can be probed by PTA data due to the dominant Domain-Wall contribution to the gravitational wave background.

Introduction.–Pulsar Timing Arrays (PTA) offer a new window to observe the universe through gravitational waves (GW) in the nano-Hertz frequency range [1–6]. A potential source of GWs at these frequencies is a population of supermassive black-hole binaries (SMBHBs) in the local universe [6, 7]. Besides, cosmic strings, which may have been produced in the early universe during a spontaneous $U(1)$ symmetry-breaking event [8–11], generate a stochastic gravitational-wave background (SGWB) down to these low frequencies as part of a vast spectrum spanning many decades in frequency; see [12, 13] for recent reviews. In fact, given the very wide and nearly scale-invariant GW spectrum from cosmic strings, the PTA limits are very relevant to anticipate the prospects for probing a cosmic-string GW signal at LISA [14] or Einstein Telescope [15]. Cosmic strings can either be *local* or *global* depending on whether the spontaneously broken symmetry is a gauge or global $U(1)$. Models of local strings have been confronted to PTA data in [16–18], and most recently to the 15-year NANOGrav (NG15) data in [5] and the EPTA data release 2 [6, 19].

This paper focuses instead on GW from global strings [12, 20–24], which were not analysed in [5]. Many Standard-Model extensions feature such additional global $U(1)$ symmetry that gets spontaneously broken at the scale f_a by the vacuum expectation value of a complex scalar field, thus delivering a Nambu-Goldstone Boson. A famous example is the Peccei-Quinn $U(1)$ symmetry advocated to solve the strong CP problem and its associated axion particle [25–28]. Because the $U(1)$ symmetry gets also broken explicitly at later times, the axion acquires a mass. At that moment, domain walls can also populate the universe [29].

This paper considers this broad class of models of so-called *Axion-Like-Particles* (ALPs) with mass m_a and decay constant f_a, corresponding to the scale of spontaneous symmetry breaking. If the cosmic-string and domain-wall formations happen before inflation, those are diluted away and become irrelevant. On the other hand, if the $U(1)$ is broken at the end or after inflation (in this case, the ALP is dubbed *post-inflationary*), cosmic strings give rise to a population of loops that generate a SGWB throughout the cosmic history. At the same time, they also generate axion particles [30–36], while domain walls bring an additional contribution to the GW spectrum [37–40].

We aim to use the most recent limits on the SGWB from NG15 data set to derive independent bounds on the parameter space of post-inflationary ALPS. Given that a GW signal has been observed [1], any further improved sensitivity from future PTA observatories will not enable pushing down the constraints. Therefore, the constraints presented in this paper on the axion mass and decay constant are not expected to change in the future by more than a factor of a few. Our approach is the following. We analyse the recent NG15 data via the code `PTArcade` [41, 42], first considering the two SGWB from global cosmic strings and domain walls without the astrophysical background. We compare the interpretation of data in terms of SMBHBs and of global cosmic strings and domain walls by calculating the Bayes factor (BF). Next, we set constraints on the new physics contribution, which leads to a SGWB that is too strong and conflicts with the data. The results of the best fit and the constraints on the SGWB from domain walls have been presented in the recent analysis with NG15 data by the NANOGrav collaboration [5]. (Refs. [43, 44] fitted the domain-wall and/or global-string signal to the IPTA DR2 and/or NANOGrav 12.5-year data however did not derive the exclusion region.) We further translate these

* geraldine.servant@desy.de
† peera.simakachorn@ific.uv.es

bounds into constraints in the ALP parameter space. In addition, this work presents a similar analysis (determining best fits and setting constraints) for global strings for the first time with NG15.

Post-inflationary axion and its GW.– The ALP can be defined as the angular mode θ of a complex scalar field $\Phi \equiv \phi \exp(i\theta)$ with ϕ the radial partner. It has the Lagrangian density, $\mathcal{L} = \frac{1}{2}\partial_\mu \Phi^* \partial^\mu \Phi - V(\Phi) - V_c$ with V_c the correction responsible for $U(1)$ symmetry restoration and trapping $\Phi \to 0$ at early times. The potential has three terms:

$$V(\Phi) = \underbrace{\frac{\lambda}{2}(\phi^2 - f_a^2)^2}_{\text{cosmic strings}} + \underbrace{\frac{m_a^2 f_a^2}{N_{\rm DW}^2}\left[1 - \cos\left(N_{\rm DW}\theta\right)\right]}_{\text{domain walls}} + V_{\rm bias},$$

where f_a is the vacuum expectation value of the field, $m_a \equiv m_a(T)$ is the axion mass, $N_{\rm DW}$ is the number of domain walls, and $V_{\rm bias}$ is some further explicit $U(1)$ breaking term. The first term is responsible for $U(1)$ spontaneous breaking, while the second and third terms explicitly break the $U(1)$. These three terms are ranked according to their associated energy scales (large to small) corresponding to their sequences in defect formations: from cosmic strings to domain walls and then their decays.

During inflation, the complex scalar field is driven to the minimum of the potential $V(\Phi)$ if $V_c \ll V(\Phi)$. Quantum fluctuations along the axion direction due to the de Sitter temperature $\mathcal{O}(H_{\rm inf})$ can generate a positive quadratic term in the potential and restore the $U(1)$ symmetry, that gets eventually broken at the end of inflation, leading to cosmic strings if $H_{\rm inf}/(2\pi f_a) \gtrsim 1$ [45–47]. However, the current CMB bound [48] on the inflationary scale $H_{\rm inf} < 6.1 \cdot 10^{13}\,\text{GeV}$ implies that f_a is too small to generate an observable cosmic-string SGWB. Still, there are several other ways in which $U(1)$ can get broken after inflation even for large f_a: *i)* A large and positive effective ϕ-mass can be generated by coupling ϕ to the inflaton χ (*e.g.,* $\mathcal{L} \supset \chi^2\phi^2$) which, for large χ, traps $\phi \to 0$ during inflation[1]. *ii)* ϕ could couple to a thermal (SM or secluded) plasma of temperature T that would generate a large thermal V_c correction, restoring the $U(1)$[2]. *iii)* Lastly, non-perturbative processes, such as preheating, could also lead to $U(1)$ restoration after inflation [51–55].

When V_c drops, the first term of $V(\Phi)$ breaks spontaneously the $U(1)$ symmetry at energy scale f_a, leading to the network formation of line-like defects or *cosmic strings* with tension $\mu = \pi f_a^2 \log\big(\lambda^{1/2} f_a/H\big)$ [11]. As $U(1)$ symmetry is approximately conserved when the axion mass is negligible, the cosmic strings survive for long and evolve into the *scaling regime* by chopping-off loops [56–69]. Loops are continuously produced and emit GW throughout cosmic history. The resulting GW signal corresponds to a SGWB that is entirely characterized by its frequency power spectrum. The later is commonly expressed as the GW fraction of the total energy density of the universe $h^2\Omega_{\rm GW}(f_{\rm GW})$. A loop population produced at temperature T quickly decays into GW of frequency [12],

$$f_{\rm GW}^{\rm cs}(T) \simeq 63\ \text{nHz}\left(\frac{\alpha}{0.1}\right)\left(\frac{T}{10\text{MeV}}\right)\left[\frac{g_*(T)}{10.75}\right]^{\frac{1}{4}}, \quad (1)$$

where $\alpha \sim \mathcal{O}(0.1)$ is the typical loop size in units of the Hubble horizon $1/H$. If the network of cosmic strings is stable until late times, *i.e.,* in the limit $m_a \to 0$, its SGWB is characterized by [12, 70],

$$h^2\Omega_{\rm GW}^{\rm cs}(f_{\rm GW}) \simeq 1.3 \cdot 10^{-9}\left(\frac{f_a}{3 \cdot 10^{15}\ \text{GeV}}\right)^4 \times \\ \times \mathcal{G}(T(f_{\rm GW}))\left[\frac{C_{\rm eff}(f_{\rm GW})}{2.24}\right]\left[\frac{\mathcal{D}(f_a, f_{\rm GW})}{94.9}\right]^3 \quad (2)$$

where $\mathcal{G}(T) \equiv [g_*(T)/g_*(T_0)][g_{*s}(T_0)/g_{*s}(T)]^{4/3}$, $\mathcal{D}(f_a, f_{\rm GW})$ is the log correction defined in footnote[3], and $C_{\rm eff}(f_{\rm GW})$ is the loop-production efficiency which also receives a small log correction originated from axion production [12]. g_* and g_{*s} measure the number of relativistic degrees of freedom in the energy and entropy densities, respectively. Note that the exponent '3' of the log-dependent term $\mathcal{D}$ is still under debate [22, 34–36, 71–78]. E.g., some numerical simulations find the scaling network leading the exponent '3' [78], and the non-scaling one leads to '4' [22, 34, 35].

As the Universe cools, the axion mass develops due to non-perturbative effects (like strong confinement in the case of the QCD axion). The second term in $V(\Phi)$ breaks explicitly the $U(1)$ discretely, leading to sheet-liked defects or *domain walls*, attached to the cosmic strings. The domain wall is characterized by its surface tension $\sigma \simeq 8 m_a f_a^2/N_{\rm DW}^2$ [79]. The axion field starts to feel the presence of the walls when $3H \simeq m_a$. The domain-wall network can be stable or unstable depending on the number of domain walls attached to a string. The value of $N_{\rm DW}$ is very UV-model-dependent. It can be linked the discrete symmetry $Z_{N_{\rm DW}}$ [80–82] that remains after the confinement of the gauge group that breaks the

[1] As the inflaton field value relates to the Hubble parameter, this mass is called *Hubble-induced* mass.

[2] For example, the KSVZ-type of interaction couples ϕ to a fermion ψ charged under some gauge symmetry with A_μ: $\mathcal{L} \supset y\phi\bar{\psi}\psi +$ h.c. $+ g\bar{\psi}\gamma^\mu\psi A_\mu$, that can generate thermal corrections: $V_c = y^2T^2\phi^2$ for $y\phi < T$ and $V_c = g^4T^4\ln(y^2\phi^2/T^2)$ for $y\phi \gtrsim T$ [49, 50]. When $V_c > \lambda f_a^4$, the ϕ-field is trapped at the origin at temperature $T \gtrsim \sqrt{\lambda} f_a/y$ for $yf_a < T$ and $T \gtrsim \lambda^{1/4} f_a/g$ for $yf_a > T$. For couplings of order unity, $f_a < T < T_{\rm max} \simeq 6.57 \cdot 10^{15}\,\text{GeV}$ is the maximum reheating temperature bounded by the inflationary scale and assuming instantaneous reheating. Nonetheless, if λ is small (corresponding to a small radial-mode mass), the bound can be weakened.

[3] $\mathcal{D}(f_a, f_{\rm GW}) = \log\left[1.7 \cdot 10^{41}\left(\frac{f_a}{3\cdot 10^{15}\,\text{GeV}}\right)\left(\frac{10\,\text{nHz}}{f_{\rm GW}}\right)^2\right]$

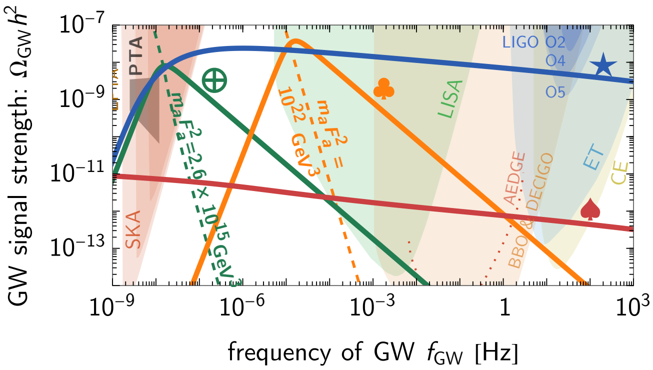

FIG. 1. SGWB from axionic strings $\{\bigstar, \spadesuit\}$ ($N_{\rm DW} = 1$) and domain walls $\{\bigoplus, \clubsuit\}$ ($N_{\rm DW} > 1$), corresponding to the benchmark points in the axion parameter space in Fig. 3 (with $T_\star = \{128\,\mathrm{MeV}, 10^2\,\mathrm{GeV}\}$ for $\{\bigoplus, \clubsuit\}$). The best-fitted spectra to the PTA data are $\bigstar$ for global strings (corresponding to $\{f_a, m_a\} \simeq \{9.9 \cdot 10^{15}$ GeV$, 4.8 \cdot 10^{-15}$ eV$\}$) and $\bigoplus$ for domain walls (with $m_a F_a^2 = 2.6 \cdot 10^{15}$ GeV^3). The power-law integrated sensitivity curves of GW experiments [14, 86–99] are taken from [12, 100]. For fixed $\{m_a, f_a\}$ values, the peak of the DW-GW spectrum moves along the dashed line as $T_\star$ varies; see Eq. (11).

global $U(1)$ symmetry explicitly and generates the axion mass. This occurs at the scale $\Lambda \simeq \sqrt{m_a F_a}$, where $F_a = f_a/N_{\rm DW}$, that is when the domain walls are generated, attaching to the existing cosmic strings.

For $N_{\rm DW} > 1$, the string-wall system is stable and long-lived. Its decay may be induced by $V_{\rm bias}$, the biased term [83–85], which could be of QCD origin [29, 39]. This decay is desirable to prevent DW from dominating the energy density of the universe at late times. $V_{\rm bias}$ is therefore an additional free parameter beyond m_a and f_a that enters the GW prediction in the case where $N_{\rm DW} > 1$.

i) $N_{\rm DW} = 1$ – If only one domain wall is attached to a string, *i.e.*, $N_{\rm DW} = 1$, the string-wall system quickly annihilates due to DW tension when[4] $H(T_{\rm dec}) \simeq m_a$ [40]. The cosmic string SGWB features an IR cut-off corresponding to the temperature

$$T_{\rm dec} \simeq 1.6\ \mathrm{MeV} \left[\frac{10.75}{g_*(T_{\rm dec})}\right]^{\frac14} \left(\frac{m_a}{10^{-15}\ \mathrm{eV}}\right)^{\frac12}, \quad (3)$$

associated with the frequency,

$$f_{\rm GW}^{\rm cs}(m_a) \simeq 9.4\ \mathrm{nHz} \left(\frac{\alpha}{0.1}\right) \left(\frac{m_a}{10^{-15}\mathrm{eV}}\right)^{\frac12}. \quad (4)$$

The cut-off position (peak frequency) and amplitude can be estimated with Eqs. (2)–(4). At $f < f_{\rm GW}^{\rm cs}(T_{\rm dec})$, the spectrum scales as $\Omega_{\rm GW} \propto f^3$ due to causality. Note that for $m_a \ll 10^{-16}$ eV, the cut-off sits at low frequencies, and within the PTA window we recover the same GW spectrum as the one in the limit $m_a \to 0$. Our analysis applies the numerical templates of the global-string SGWB – covering the ranges of f_a and $T_{\rm dec}$ priors. We calculated these templates numerically by solving the string-network evolution via the *velocity-dependent one-scale* (VOS) model [62, 102–105] and calculating the SGWB following Ref. [12].

ii) $N_{\rm DW} > 1$ – Attached to a string, $N_{\rm DW}$ walls balance among themselves and prevent the system from collapsing at $H \simeq m_a$ [40, 106]. The domain-wall network later evolves to the *scaling regime* where there is a constant number of DW per comoving volume $\mathcal{V} \simeq H^{-3}$. The energy density of DW is $\rho_{\rm DW} \simeq \sigma H^{-2}/\mathcal{V} \simeq \sigma H$ and it acts as a long-lasting source of SGWB [83, 107–112]; *cf.* [113] for a compact review. The network red-shifts slower than the Standard Model (SM) radiation energy density and could dominate the universe. The biased term $V_{\rm bias}$ – describing the potential difference between two consecutive vacua – explicitly breaks the $U(1)$ symmetry and induces the pressure on one side of the wall [8, 83]. Once this pressure overcomes the tension of the wall[5], the string-wall system collapses at temperature,

$$T_\star \simeq 53\mathrm{MeV} \left[\frac{10.75}{g_*(T_*)}\right]^{\frac14} \left[\frac{V_{\rm bias}^{\frac14}}{10\mathrm{MeV}}\right]^2 \left[\frac{\mathrm{GeV}}{m_a}\right]^{\frac12} \left[\frac{10^6\mathrm{GeV}}{f_a/N_{\rm DM}}\right]. \quad (5)$$

The fraction of energy density in DW is maximized at this time and reads,

$$\begin{aligned} \alpha_\star &\equiv \rho_{\rm DW}/\rho_{\rm tot}(T_\star) \simeq \sigma H/(3M_{\rm Pl}^2 H^2(T_\star)), \\ &\simeq 4 \cdot 10^{-4} \left[\frac{10.75}{g_*(T_\star)}\right]^{\frac12} \left[\frac{m_a}{\mathrm{GeV}}\right] \left[\frac{f_a/N_{\rm DW}}{10^6\mathrm{GeV}}\right]^2 \left[\frac{50\mathrm{MeV}}{T_\star}\right]^2. \end{aligned} \quad (6)$$

The energy density emitted in GW is [79]

$$\rho_{\rm GW}/\rho_{\rm tot} \sim \frac{3}{32\pi}\epsilon\alpha_\star^2 \quad (7)$$

where we fix $\epsilon \simeq 0.7$ from numerical simulations [111]. It reaches its maximum at $T_\star$. The spectrum exhibits the broken-power law shape and reads,

$$\begin{aligned} h^2\Omega_{\rm GW}^{\rm dw}(f_{\rm GW}) \simeq & 7.35 \cdot 10^{-11} \left[\frac{\epsilon}{0.7}\right] \left[\frac{g_*(T_\star)}{10.75}\right] \left[\frac{10.75}{g_{*s}(T_\star)}\right]^{\frac43} \times \\ & \times \left(\frac{\alpha_\star}{0.01}\right)^2 \mathcal{S}\left(\frac{f_{\rm GW}}{f_{\rm p}^{\rm dw}}\right) \end{aligned} \quad (8)$$

[4] The string tension loses against the DW surface tension at time $t_{\rm dec}$ defined by [101] $F_{\rm str} \sim \mu/R_{\rm dec} \simeq \sigma \Rightarrow R_{\rm dec} \sim H^{-1}(t_{\rm dec}) \sim \mu/\sigma \sim m_a^{-1}$ where R is the string curvature, assumed to be of Hubble size.

[5] The pressure from $V_{\rm bias}$ is $p_V \sim V_{\rm bias}$, while the wall's tension reads $p_T \sim \sigma H$ assuming the wall of horizon size. The collapse happens when $p_V > p_T$.

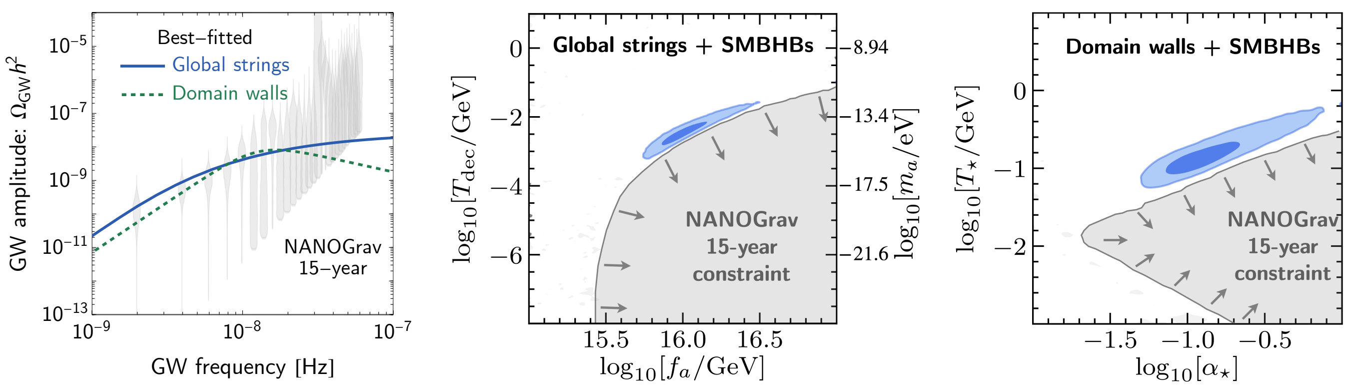

FIG. 2. *left:* The SGWB spectra from global strings and domain walls + SMBHBs, providing the best-fits to the PTA data and corresponding to $\{f_a, m_a\} \simeq \{9.9 \cdot 10^{15}\ \mathrm{GeV}, 4.8 \cdot 10^{-15}\ \mathrm{eV}\}$ for global strings and $m_a F_a^2 = 2.6 \cdot 10^{15}\ \mathrm{GeV}^3$ for domain walls (in violins, taken from [5]). *middle and right:* 1σ (dark blue) and 2σ (light blue) regions of the likelihood of the global-string/domain-wall parameters, assuming the template of global-string/domain-wall + SMBHB backgrounds. The gray region is excluded due to too strong GW signals from global strings/domain walls that are in conflict with PTA data.

where the normalized spectral shape is,

$$\mathcal{S}(x) = (3+\beta)^\delta / (\beta x^{-\frac{3}{\delta}} + 3x^{\frac{\beta}{\delta}})^\delta. \tag{9}$$

The f^3-IR slope is dictated by causality, the UV slope f^β is model-dependent, and the width of the peak is δ. The peak frequency corresponds to the DW size at $H_\star$, *i.e.,* the horizon size $f^\star_{\rm GW} \sim H^{-1}$ [111]. Its value today reads,

$$f_{\rm p}^{\rm dw} \simeq 1.14 \mathrm{nHz} \left[\frac{g_*(T_\star)}{10.75}\right]^{\frac{1}{2}} \left[\frac{10.75}{g_{*s}(T_\star)}\right]^{\frac{1}{3}} \left[\frac{T_\star}{10 \mathrm{MeV}}\right]. \tag{10}$$

From Eqs. (6), (8), and (10), each value of $m_a f_a^2$ corresponds to a degenerate peak position of the GW spectrum,

$$h^2 \Omega_{\rm GW}^{\rm dw}(f_{\rm p}^{\rm dw}) \simeq 1.2 \cdot 10^{-10} \left[\frac{\epsilon}{0.7}\right] \left[\frac{g_*(T_\star)}{10.75}\right]^3 \left[\frac{10.75}{g_{*s}(T_\star)}\right]^{\frac{8}{3}} \times \\ \times \left[\frac{m_a}{\mathrm{GeV}}\right]^2 \left[\frac{f_a}{10^6 \mathrm{GeV}}\right]^4 \left[\frac{\mathrm{nHz}}{f_{\rm p}^{\rm dw}}\right]^4, \tag{11}$$

which are shown as the dashed-line in Fig. 1.

The DW can decay into axions, which either behave as dark radiation or decay into SM particles. When DW decay into dark radiation, the $\Delta N_{\rm eff}$ puts a bound $\alpha_\star \lesssim 0.06$ [43], *i.e.,* the peak of GW spectrum has $h^2\Omega_{\rm GW} \lesssim 10^{-9}$ (which cannot fit the whole 14 bins of NG15 data). As $\alpha_\star$ controls the amplitude of the GW spectrum (8), we consider a larger range of $\alpha_\star$, up to $\alpha_\star = 1$ when the energy density of DW starts to dominate the universe. To get around the $\Delta N_{\rm eff}$ bound, we will therefore consider the case where the axions produced by domain walls eventually decay into SM particles.

In this *paper*, we confront the most recent PTA data to both cases: *i)* $N_{\rm DW} = 1$ where the SGWB in the PTA range dominantly comes from the cosmic strings, and *ii)* $N_{\rm DW} > 1$ where the SGWB in the PTA range comes from the domain walls. These two cases correspond to axions of two utterly different mass ranges. For case *i)*, the cosmic strings live long; that is, m_a is small. Instead, the case *ii)* corresponds to the large m_a region. We compare the GW spectra in Fig. 1 for different benchmark points. Their location in the m_a, F_a plane is shown in Fig. 3.

Searching and constraining SGWB with PTA.– This work analyses the recent NG15 data set [115] covering a period of observation $T_{\rm obs} = 16.03$ years [1]. From the pulsars timing residuals, the posterior probability distributions of the global-string and domain-wall model parameters are derived. We consider 14 frequency bins of NG15 data, where the first and last bins are at $1/T_{\rm obs} \simeq 1.98$ nHz and $14/T_{\rm obs} \simeq 27.7$ nHz, respectively. The analysis is done by using `ENTERPRISE` [116, 117] via the handy wrapper `PTArcade` [41, 42]. The priors for the model parameters are summarized in Tab. I in Appendix A. We refer readers to [5] for a short review of Bayesian analysis.

This work considers the SGWB in the two scenarios discussed above, together with the astrophysical background. Fig. 2-middle and -right show the 68%-CL (or 1σ) and 95%-CL (or 2σ) in dark and light blue regions, respectively. We obtain the best-fit values $f_a = 9.87^{+2.67}_{-2.02} \cdot 10^{15}$ GeV and $T_{\rm dec} = 3.50^{+2.44}_{-1.48}$ MeV for global strings, and $\alpha_\star = 0.114^{+0.060}_{-0.033}$ and $T_\star = 128^{+55}_{-33}$ MeV for domain walls. The global-string and domain-wall SGWB are preferred over the SMBHB signal implemented by `PTArcade`, as suggested by their Bayes Factors (BF) larger than unity ($\mathrm{BF}_{\rm cs} = 26.0$, $\mathrm{BF}_{\rm dw} = 44.7$) when compared to the SMBHB interpretation; *cf.* Eq. (9) of [5]. We show the best-fitted spectra for these two new-physics cases in Fig. 2-left. Translating into axion parameters via Eq. (3) and (6), the best fits correspond to $\{f_a, m_a\} = \{9.87 \cdot 10^{15}\ \mathrm{GeV}, 4.78 \cdot 10^{-15}\ \mathrm{eV}\}$ for global strings and $m_a F_a^2 = 2.6 \cdot 10^{15}\ \mathrm{GeV}^3$ for domain walls. For completeness, we show the case without the SMBHB contribution in App. B. Because the two new-physics cases explain the data well by themselves, we see that the 1σ

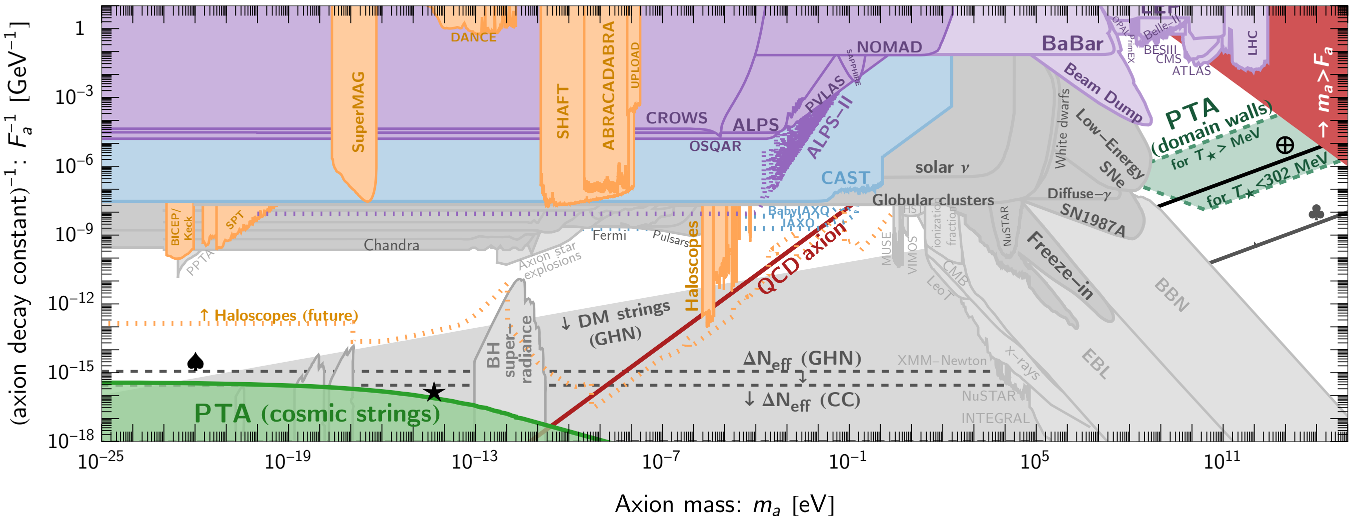

FIG. 3. PTA limits (in green) on post-inflationary axions, compared to existing experimental constraints as compiled from `AxionLimits` [114] and to theoretical bounds: dark radiation overabundance $\Delta N_{\rm eff}$ bound (12) as dashed horizontal line and ALP overabundance (13) in the shaded grey region. $F_a = f_a/N_{\rm DW}$. The comparison with experimental bounds uses $g_{\theta\gamma\gamma} = 1.02\alpha_{\rm EM}/(2\pi F_a) \approx 2.23 \cdot 10^{-3}/F_a$ for the relation between the photon coupling and F_a, as motivated by KSVZ models. The recent PTA data [1] excludes the **green** small-m_a region due to cosmic-string SGWB ($N_{\rm DW} = 1$). It also potentially excludes the high-m_a region due to domain-wall SGWB for $N_{\rm DW} > 1$, depending on the value of $T_\star$. The **other green** band at large m_a is the region that can be constrained by PTA if $T_\star$ varies in the range MeV $< T_\star <$ 302 MeV, as illustrated in Fig. 4. The two benchmark points {★, ♠} correspond to cosmic-string SGWB, and the two black benchmark lines {⊕, ♣} correspond to the domain-wall SGWB, whose spectra are shown in Fig. 1.

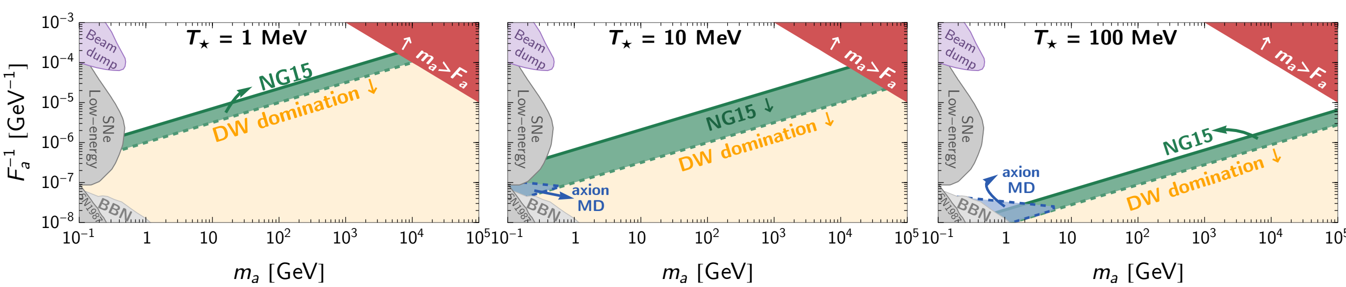

FIG. 4. The PTA-DW constraint (in **green**) changes with $T_\star$. For fixed $T_\star$ and m_a, the constrained range of F_a in **green** is derived from the $\alpha_\star$ constrained region of Fig. 2-right, using Eq. (6). The **yellow** region corresponds to $\alpha_\star > 1$ which corresponds to the DW domination and can change the GW prediction; we do not extend the constraint into this region. For $T_\star \gtrsim 302$ MeV (*cf.* Fig. 2-right), NG15 data constrains $\alpha_\star > 1$; that is, the green band overlaps part of the yellow region. The **blue** region is where the axions – produced from DW annihilations – dominate the universe before they decay prior to BBN. In this case, the theoretical prediction for the GW spectrum also has to be re-evaluated.

and 2σ regions of Fig. 2 match those without the SMBHB in Fig. 5. The values of the best fits, given in App. B, only change slightly.

Although the two scenarios could by themselves explain the signal, this work aims at setting bounds on the model parameter space that is associated with a too strong SGWB in conflict with the NG15 data. Following [5], we identify excluded regions of the new-physics parameter spaces by using the posterior-probability ratio (or K-ratio). Specifically, the excluded gray regions in Fig. 2-middle and -right correspond to the areas of parameter spaces where the K-ratio between the combined new-physics+SMBHB and the SMBHB-only models drops below 0.1[6], according to Jeffrey's scale [118], due to a too-strong SGWB from the new-physics model. We emphasize that the values of the BFs strongly depend on the modeling of the SMBHB signal as it is the ratio of evidence of the considered model and the SMBHB template. However, the constrained regions depend only slightly on it [5]. Now we discuss, in turn, the NG15 constraints for each case.

Result i) $N_{\rm DW} = 1$, implications for light ax-

[6] *i.e.*, the new-physics contribution makes the overall signal *strongly disfavored* by the data

ions– We fit the PTA data with the global-string SGWB, varying $\{f_a, T_{\rm dec}\}$. The 2D posterior result is shown in Fig. 2, and the dark-blue region is where the cosmic-string SGWB dominates and fits the data to the significance of 1σ with the best fit $\{f_a, m_a\} \simeq \{9.9 \cdot 10^{15}\ {\rm GeV}, 4.8 \cdot 10^{-15}\ {\rm eV}\}$, shown as the benchmark case $\star$ in Figs. 1 and 3. A too-large global-string SGWB is constrained by PTA in the grey region of Fig. 2-middle. For small f_a, the GW from cosmic strings cannot fit the data as its amplitude becomes too small.

As $T_{\rm dec} \ll 0.1$ MeV ($m_a \ll 10^{-17}$ eV), the cut-off (4) associated with $T_{\rm dec}$ moves below the PTA window ($f_{\rm GW}(T_{\rm dec}) <$ nHz). The constraint in this case in Fig. 2-middle reads $f_a < 2.8 \times 10^{15}$ GeV (m_a-independent), which is stronger than the LIGO bound[7] ($f_a \lesssim 8 \times 10^{16}$ GeV). For completeness, we also did the analysis for stable global strings (*i.e.,* $m_a \to 0$) in App. C, and we obtained a similar bound. For $T_{\rm dec} \gg 0.1$ MeV ($m_a \gg 10^{-17}$ eV), the cut-off sits at a frequency higher than the PTA window, and the SGWB signal is dominated by the IR tail signal, which scales as $\Omega_{\rm GW} \propto f^3$. From Eqs. (1) and (2), we obtain the asymptotic behavior of $T_{\rm dec} \propto f_a^{4/3}$ (or $m_a \propto f_a^{8/3}$), up to the log correction in Eq. (2), toward large f_a limit. We show this bound in the usual axion parameter space in the *bottom-left* corner of Fig. 3. The constraint on f_a values for $N_{\rm DW} = 1$ corresponds to $f_a > H_{\rm inf}/(2\pi)$. Therefore, it does not apply to cosmic strings linked to quantum fluctuations during inflation.

$\Delta N_{\rm eff}$ & dark matter constraints.–Although the PTA constraint excludes a large region of the axion parameter space, there exist other theoretical bounds. Axionic strings are known to emit axion particles dominantly [30]. Depending on its mass, the axion can contribute to either dark radiation or cold dark matter. Axions that are relativistic at the time of Big Bang Nucleosynthesis (BBN) are subject to the dark radiation bound expressed as a bound on the number of extra neutrino species, $\Delta N_{\rm eff} < 0.46$ [119]. There are uncertainties in deriving this bound linked to the log-correction to the number of strings in the global-string network evolution [34–36, 78]. In this paper, we quote two bounds: the one relying on the semi-analytic calculation [21] by Chang and Cui (CC), and the lattice result [22] by Gorghetto, Hardy, and Nicolaescu (GHN):

$$f_a \lesssim 10^{15}\ {\rm GeV} \left[\frac{\Delta N_{\rm eff}}{0.46}\right]^{\frac{1}{2}} \cdot \begin{cases} 3.5 & \text{(CC)}, \\ 0.88 \left[\frac{90}{\log\left(\frac{f_a}{H_{\rm BBN}}\right)}\right]^{3/2} & \text{(GHN)}, \end{cases} \tag{12}$$

where we implicitly assume $\lambda \sim 1$ for the GHN bound and $H_{\rm BBN} \simeq 4.4 \cdot 10^{-25}$ GeV is the Hubble parameter at BBN scale ($T_{\rm BBN} \simeq$ MeV). Since ALPs have a small mass at late times, they behave as cold dark matter. Subject to the uncertainty in simulations [22, 36, 75], the abundance Ω_a of axion dark matter from strings predicted by GHN sets a constraint on the axion,

$$f_a \lesssim 1.8 \cdot 10^{15}\ {\rm GeV} \sqrt{\left[\frac{\Omega_a}{0.266}\right]\left[\frac{25 \cdot x_{0,a}}{\xi_* \cdot 10}\right]\left[\frac{g_*(T_{\rm dec})}{3.5}\right]^{1/4}} \times \\ \times \sqrt{\left[\frac{10^2}{\log(f_a/m_a)}\right]\left[\frac{10^{-22}{\rm eV}}{m_a}\right]^{1/2}}, \tag{13}$$

typically $\xi_* \approx 25$ and $x_{0,a} \approx 10$ [22]. Note that the collapse of the string-wall system at $H \simeq m_a$ produces an axion abundance of the same order as the one from strings [35], therefore an $\mathcal{O}(1)$ correction is expected in Ω_a in Eq. 13. We show both dark radiation and dark matter bounds in Fig. 3. We see that the PTA constraint becomes competitive to the equivocal $\Delta N_{\rm eff}$ bound for $m_a \lesssim 10^{(-22,-23)}$ eV.

Effects of non-standard cosmology.–So far, the standard ΛCDM cosmology [119] has been assumed. On the other hand, alternative expansion histories to the usually assumed radiation era are not unlikely above the BBN scale, such as a period of matter domination or kination resulting in a strongly different spectrum of GW for cosmc strings[12, 20, 21, 70, 120]. Nonetheless, the non-standard cosmology modifies the CS-GW spectrum in the high-frequency direction. From Eq. (1), the non-standard era must end below the MeV scale to substantially change the SGWB in the PTA window. We have checked the effects of matter and kination eras with `PTArcade` and found that such SGWB distortion cannot improve the global string interpretation of PTA data. Besides, we expect only a negligible effect on the PTA bound obtained in this work.

QCD axion.–From Fig. 3, the PTA data can exclude some part of the QCD axion (red line). However, this region of parameter space is already excluded due to overabundance of axion DM or due to $\Delta N_{\rm eff}$ bounds. To relax these bounds, one can invoke a scenario where cosmic strings decay during a matter-domination era (or any era with the equation-of-state smaller than that of radiation), which efficiently dilutes these relics but still allow for a GW signal in the PTA frequency range [23, 24]. Interestingly, such matter-domination era at early times can imprint a specific signature in the SGWB from global strings, which can be observed in future-planned GW experiments at frequencies above nHz frequencies[12, 20, 21, 121].

Result ii) $N_{\rm DW} > 1$, implications for heavy axions.– We fit the DW SGWB, varying $\{T_\star, \alpha_\star, \beta, \delta\}$ to the PTA data. Because the posteriors of β and δ are unconstrained, we show only the 2D posterior of $\{T_\star, \alpha_\star\}$ in Fig. 2-right. The DW SGWB can fit the PTA data in the dark-blue region to 1σ. The best fit value of $\{T_\star, \alpha_\star\}$ is translated via Eq. (6) into $m_a F_a^2 \simeq 2.6 \times 10^{15}$ GeV and corresponds to the benchmark spectrum and line in

[7] Derived by solving numerically Eq. (2) with $f_{\rm GW} \simeq 20$ Hz and $h^2\Omega_{\rm GW} \simeq 10^{-8}$ for LIGO.

Figs. 1 and 3, respectively. However, for large enough $\alpha_\star$, DW generates a GW signal well stronger than the PTA signal, leading to a constraint in the gray region in Fig.2-right. The constraint is the strongest $\alpha_\star \lesssim 0.02$ at $T_\star \simeq 13.8$ MeV when the peak of the SGWB is centered in the PTA window; see also Eq. (10). For $T_\star > 13.8$ MeV (< 13.8 MeV), the GW spectrum has its IR (UV) tail in the PTA range; thus, the constraint on $\alpha_\star$ becomes weaker.

For heavy axions with $Z_{N_{\rm DW}}$-symmetry whose mass depends on the explicit-symmetry-breaking scale $\Lambda \simeq \sqrt{m_a F_a}$ where $F_a = f_a/N_{\rm DW}$, the PTA constraint in Fig. 2-right is translated via Eq. (6) into a bound on $\{F_a, m_a\}$ with the degeneracy among them. For a fixed $T_\star$, we obtain the excluded region on the axion parameter space, as shown in the green region of Fig. 4. Very large f_a corresponds to $\alpha_\star > 1$; the DW-domination era occurs before it decays and should affect the GW prediction. We do not extend our PTA bound in the DW domination regime, shown in the yellow of Fig. 4. In fact, Eq. (8) assumes a radiation-dominated universe. To constrain the DW-domination region requires computing the evolution of the DW network and its SGWB in a universe with a modified equation of state. This is a non-trivial task which we leave for future investigation; see also [122]. To be conservative, we leave this region unconstrained for now, although we expect some constraints will prevail there.

Because the PTA constraint on $\alpha_\star$ is not linear in $T_\star$, the width of the PTA band is maximized only for $T_\star \simeq 13.8$ MeV where the bound on $\alpha_\star$ is the strongest. In Fig. 3, we also show the ability to constrain axion parameter space with the PTA-DW signal. We obtain the constraint by summing the excluded regions for the range MeV $\leq T_\star \lesssim 302\,\text{MeV}$, where $T_\star \simeq 302\,\text{MeV}$ is where the constraint has $\alpha_\star \geq 1$ in Fig. 2-right. The upper limit of the green region (large-m_a) of Fig. 3 is set by the constraint at $T_\star =$ MeV: $\alpha_\star \gtrsim 0.2$; see Fig. 2-right. Using Eq. (6), this upper bound is defined as $m_a F_a^2 \gtrsim 2 \cdot 10^{11}$ GeV^3. Some part of the white region above the green band (smaller $m_a F_a^2$) will be probed by future particle physics experiments [123–126].

Other than the PTA bound, the $\{T_\star, \alpha_\star\}$ parameter space is subject to theoretical constraints related to the DW decay and its by-products. In this work, we consider that the heavy axion produced from the DW decay subsequently decays into SM particles, *e.g.,* photons via $\mathcal{L} \supset -\frac{g}{4} F\tilde{F}\theta$ with the decay rate $\Gamma_{\theta\gamma} = m_a^3 g^2/(64\pi)$ [127]. Using this to $F_a = 1.92\alpha_{\rm EM}/(2\pi g_{\theta\gamma})$, the decay is efficient when $\Gamma_{\theta\gamma} > H(T)$, which is equivalent to,

$$T < T_{\theta\gamma} \equiv 236\,\text{MeV} \left[\frac{10.75}{g_*(T_{\theta\gamma})}\right]^{\frac{1}{4}} \left[\frac{m_a}{\text{GeV}}\right]^{\frac{3}{2}} \left[\frac{10^6\ \text{GeV}}{f_a/N_{\rm DW}}\right]. \tag{14}$$

This bound is similar to the BBN bound from [128] in Figs.3–4. Moreover, the heavy axion might decay after it dominates the universe if $T_\star > T_{\theta\gamma}$ and $T_{\theta\gamma} < T_{\rm dom}$ where the temperature $T_{\rm dom}$ corresponds to the heavy-axion domination, *i.e.,* $\rho_a(T_{\rm dom}) = \rho_a(T_\star)(a_\star/a_{\rm dom})^3 = \rho_{\rm tot}(T_{\rm dom})$,

$$T_{\rm dom} \simeq 0.02\ \text{MeV} \left[\frac{10.75}{g_*(T)}\right]^{\frac{1}{2}} \left[\frac{50\text{MeV}}{T_\star}\right] \left[\frac{m_a}{\text{GeV}}\right] \left[\frac{f_a/N_{\rm DW}}{10^6\text{GeV}}\right]^2. \tag{15}$$

This heavy axion induces a matter-domination era that would change the GW prediction, *e.g.,* the IR tail of the spectrum gets distorted by the modified equation-of-state of the universe [129–131]. We mark this region in the blue region of Fig. 4. For the sum of PTA constraints varying $T_\star$ in Fig. 3, we omit the axion-MD region, which cuts the PTA region from the low-m_a region[8].

Other effects.–The friction from axionic DW interactions with particles of the thermal plasma could change the dynamics [132] and potentially the SGWB spectrum. Another effect that could change the bounds is the potential collapse of DW into primordial black holes [133–135]. Nonetheless, since the prediction is based on the spherical collapse, we would need a large scale numerical of DW to check whether the PBH formation can be realized. Lastly, further QCD effects can impact the DW decays relevant for PTA [122, 136, 137].

Conclusion.– We analysed the consequences of the 15-year NANOGrav data on the parameter space of post-inflationary axions. The bounds in Fig. 3 come in two distinct regimes: the low and large axion mass ranges, which are respectively associated with signals from axionic global strings ($N_{\rm DW} = 1$) and domain walls ($N_{\rm DW} > 1$). In the low-axion-mass region, the constraint on f_a is strongest for $m_a \ll 10^{-17}$ eV, and reads $f_a < 2.8 \times 10^{15}$ GeV. It is competitive with the $\Delta N_{\rm eff}$ bound. At high masses, 0.1 GeV $\lesssim m_a \lesssim 1000$ TeV, a substantial region, corresponding to $m_a(f_a/N_{\rm DW})^2 \gtrsim 2 \times 10^{11}$ GeV^3, can be excluded for DW decaying in the $T_* \propto \sqrt{V_{\rm bias}} \sim$ 1-300 MeV range.

This study motivates the investigation of the SGWB in the regime of DW domination as this knowledge could lead to substantial new constraints at large m_a and f_a values. Once the network of DW dominates the universe, the scaling regime might be lost. DW would instead enter the stretching regime [138] where the energy density scales as $\rho \propto a^{-1}$, the equation of state of $-2/3$ leading to the accelerated cosmic expansion could be in tension with several cosmological observations [122, 139]. Moreover, a period of early DW domination can also occur and affect the SGWB spectrum [12, 140, 141].

To conclude, GW are a promising tool to probe axion physics. PTA measurements have opened the possibility to observe the universe at the MeV scale, enabling to constrain several classes of axion models. By combining

[8] Using Eq. (6) with $\alpha_\star = 1$ and $T_{\theta\gamma} < T_{\rm dom}$, the cut follows $236(m_a/\text{GeV}) < (F_a/10^6\text{GeV})^2$.

NG15 with other data sets from EPTA, InPTA, PPTA, and CPTA collaborations, the constraints on axions can become more stringent, similarly to what has been shown for other cosmological sources [142, 143]. Other planned GW observatories will permit the search for different parts of the predicted SGWB from axion physics and distinguish them from other SGWB from astrophysical and cosmological sources [144].

Acknowledgement.– We are indebted to Andrea Mitridate for teaching us `PTArcade` and for his substantial help on the analysis. We thank Marco Gorghetto for discussions and Matthias Koschnitzke for his technical support. PS is funded by Generalitat Valenciana grant PROMETEO/2021/083. This work is supported by the Deutsche Forschungsgemeinschaft under Germany's Excellence Strategy – EXC 2121 ,,Quantum Universe" – 390833306 and the Maxwell computational resources operated at Deutsches Elektronen-Synchrotron (DESY), Hamburg, Germany.

---

[1] NANOGrav collaboration, *The NANOGrav 15-year Data Set: Evidence for a Gravitational-Wave Background*, *Astrophys. J. Lett.* **951** (2023) [2306.16213].

[2] J. Antoniadis et al., *The second data release from the European Pulsar Timing Array III. Search for gravitational wave signals*, 2306.16214.

[3] D. J. Reardon et al., *Search for an isotropic gravitational-wave background with the Parkes Pulsar Timing Array*, *Astrophys. J. Lett.* **951** (2023) [2306.16215].

[4] H. Xu et al., *Searching for the Nano-Hertz Stochastic Gravitational Wave Background with the Chinese Pulsar Timing Array Data Release I*, *Res. Astron. Astrophys.* **23** (2023) 075024 [2306.16216].

[5] NANOGrav collaboration, *The NANOGrav 15-year Data Set: Search for Signals from New Physics*, *Astrophys. J. Lett.* **951** (2023) [2306.16219].

[6] J. Antoniadis et al., *The second data release from the European Pulsar Timing Array: V. Implications for massive black holes, dark matter and the early Universe*, 2306.16227.

[7] NANOGrav collaboration, *The NANOGrav 15-year Data Set: Constraints on Supermassive Black Hole Binaries from the Gravitational Wave Background*, 2306.16220.

[8] T. W. B. Kibble, *Topology of Cosmic Domains and Strings*, *J. Phys. A* **9** (1976) 1387.

[9] T. W. B. Kibble, *Some Implications of a Cosmological Phase Transition*, *Phys. Rept.* **67** (1980) 183.

[10] M. B. Hindmarsh and T. W. B. Kibble, *Cosmic Strings*, *Rept. Prog. Phys.* **58** (1995) 477 [hep-ph/9411342].

[11] A. Vilenkin and E. P. S. Shellard, *Cosmic Strings and Other Topological Defects*. Cambridge University Press, 7, 2000.

[12] Y. Gouttenoire, G. Servant and P. Simakachorn, *Beyond the Standard Models with Cosmic Strings*, *JCAP* **07** (2020) 032 [1912.02569].

[13] P. Auclair et al., *Probing the gravitational wave background from cosmic strings with LISA*, *JCAP* **04** (2020) 034 [1909.00819].

[14] LISA Cosmology Working Group collaboration, *Cosmology with the Laser Interferometer Space Antenna*, 2204.05434.

[15] M. Maggiore et al., *Science Case for the Einstein Telescope*, *JCAP* **03** (2020) 050 [1912.02622].

[16] J. Ellis and M. Lewicki, *Cosmic String Interpretation of NANOGrav Pulsar Timing Data*, *Phys. Rev. Lett.* **126** (2021) 041304 [2009.06555].

[17] S. Blasi, V. Brdar and K. Schmitz, *Has NANOGrav found first evidence for cosmic strings?*, *Phys. Rev. Lett.* **126** (2021) 041305 [2009.06607].

[18] W. Buchmuller, V. Domcke and K. Schmitz, *From NANOGrav to LIGO with metastable cosmic strings*, *Phys. Lett. B* **811** (2020) 135914 [2009.10649].

[19] EPTA collaboration, *Practical approaches to analyzing PTA data: Cosmic strings with six pulsars*, 2306.12234.

[20] C.-F. Chang and Y. Cui, *Stochastic Gravitational Wave Background from Global Cosmic Strings*, *Phys. Dark Univ.* **29** (2020) 100604 [1910.04781].

[21] C.-F. Chang and Y. Cui, *Gravitational waves from global cosmic strings and cosmic archaeology*, *JHEP* **03** (2022) 114 [2106.09746].

[22] M. Gorghetto, E. Hardy and H. Nicolaescu, *Observing invisible axions with gravitational waves*, *JCAP* **06** (2021) 034 [2101.11007].

[23] N. Ramberg and L. Visinelli, *Probing the Early Universe with Axion Physics and Gravitational Waves*, *Phys. Rev. D* **99** (2019) 123513 [1904.05707].

[24] N. Ramberg and L. Visinelli, *QCD axion and gravitational waves in light of NANOGrav results*, *Phys. Rev. D* **103** (2021) 063031 [2012.06882].

[25] R. D. Peccei and H. R. Quinn, *CP Conservation in the Presence of Instantons*, *Phys. Rev. Lett.* **38** (1977) 1440.

[26] R. D. Peccei and H. R. Quinn, *Constraints Imposed by CP Conservation in the Presence of Instantons*, *Phys. Rev. D* **16** (1977) 1791.

[27] S. Weinberg, *A New Light Boson?*, *Phys. Rev. Lett.* **40** (1978) 223.

[28] F. Wilczek, *Problem of Strong P and T Invariance in the Presence of Instantons*, *Phys. Rev. Lett.* **40** (1978) 279.

[29] P. Sikivie, *Of Axions, Domain Walls and the Early Universe*, *Phys. Rev. Lett.* **48** (1982) 1156.

[30] R. L. Davis, *Cosmic Axions from Cosmic Strings*, *Phys. Lett. B* **180** (1986) 225.

[31] R. L. Davis and E. P. S. Shellard, *DO AXIONS NEED INFLATION?*, *Nucl. Phys. B* **324** (1989) 167.

[32] A. Dabholkar and J. M. Quashnock, *Pinning Down the Axion*, *Nucl. Phys. B* **333** (1990) 815.

[33] R. A. Battye and E. P. S. Shellard, *Global string radiation*, *Nucl. Phys. B* **423** (1994) 260 [astro-ph/9311017].

[34] M. Gorghetto, E. Hardy and G. Villadoro, *Axions from Strings: the Attractive Solution*, *JHEP* **07** (2018)

151 [1806.04677].

[35] M. Gorghetto, E. Hardy and G. Villadoro, *More axions from strings*, SciPost Phys. **10** (2021) 050 [2007.04990].

[36] M. Buschmann, J. W. Foster, A. Hook, A. Peterson, D. E. Willcox, W. Zhang et al., *Dark matter from axion strings with adaptive mesh refinement*, Nature Commun. **13** (2022) 1049 [2108.05368].

[37] D. H. Lyth, *Estimates of the cosmological axion density*, Phys. Lett. B **275** (1992) 279.

[38] M. Nagasawa and M. Kawasaki, *Collapse of axionic domain wall and axion emission*, Phys. Rev. D **50** (1994) 4821 [astro-ph/9402066].

[39] S. Chang, C. Hagmann and P. Sikivie, *Studies of the motion and decay of axion walls bounded by strings*, Phys. Rev. D **59** (1999) 023505 [hep-ph/9807374].

[40] T. Hiramatsu, M. Kawasaki, K. Saikawa and T. Sekiguchi, *Production of dark matter axions from collapse of string-wall systems*, Phys. Rev. D **85** (2012) 105020 [1202.5851].

[41] A. Mitridate, *PTArcade*, .

[42] A. Mitridate, D. Wright, R. von Eckardstein, T. Schröder, J. Nay, K. Olum et al., *PTArcade*, 2306.16377.

[43] R. Z. Ferreira, A. Notari, O. Pujolas and F. Rompineve, *Gravitational waves from domain walls in Pulsar Timing Array datasets*, JCAP **02** (2023) 001 [2204.04228].

[44] E. Madge, E. Morgante, C. P. Ibáñez, N. Ramberg and S. Schenk, *Primordial gravitational waves in the nano-Hertz regime and PTA data – towards solving the GW inverse problem*, 2306.14856.

[45] T. S. Bunch and P. C. W. Davies, *Quantum Field Theory in de Sitter Space: Renormalization by Point Splitting*, Proc. Roy. Soc. Lond. A **360** (1978) 117.

[46] A. D. Linde, *INFLATION CAN BREAK SYMMETRY IN SUSY*, Phys. Lett. B **131** (1983) 330.

[47] A. A. Starobinsky and J. Yokoyama, *Equilibrium state of a selfinteracting scalar field in the De Sitter background*, Phys. Rev. D **50** (1994) 6357 [astro-ph/9407016].

[48] Planck collaboration, *Planck 2018 results. X. Constraints on inflation*, Astron. Astrophys. **641** (2020) A10 [1807.06211].

[49] K. Mukaida and K. Nakayama, *Dynamics of Oscillating Scalar Field in Thermal Environment*, JCAP **01** (2013) 017 [1208.3399].

[50] K. Mukaida and K. Nakayama, *Dissipative Effects on Reheating After Inflation*, JCAP **03** (2013) 002 [1212.4985].

[51] L. Kofman, A. D. Linde and A. A. Starobinsky, *Nonthermal phase transitions after inflation*, Phys. Rev. Lett. **76** (1996) 1011 [hep-th/9510119].

[52] I. I. Tkachev, *Phase transitions at preheating*, Phys. Lett. B **376** (1996) 35 [hep-th/9510146].

[53] S. Kasuya and M. Kawasaki, *Can topological defects be formed during preheating?*, Phys. Rev. D **56** (1997) 7597 [hep-ph/9703354].

[54] S. Kasuya and M. Kawasaki, *Topological defects formation after inflation on lattice simulation*, Phys. Rev. D **58** (1998) 083516 [hep-ph/9804429].

[55] I. Tkachev, S. Khlebnikov, L. Kofman and A. D. Linde, *Cosmic strings from preheating*, Phys. Lett. B **440** (1998) 262 [hep-ph/9805209].

[56] T. W. B. Kibble, *Evolution of a System of Cosmic Strings*, Nucl. Phys. B **252** (1985) 227.

[57] A. Albrecht and N. Turok, *Evolution of Cosmic Strings*, Phys. Rev. Lett. **54** (1985) 1868.

[58] D. P. Bennett and F. R. Bouchet, *Evidence for a Scaling Solution in Cosmic String Evolution*, Phys. Rev. Lett. **60** (1988) 257.

[59] D. P. Bennett and F. R. Bouchet, *Cosmic String Evolution*, Phys. Rev. Lett. **63** (1989) 2776.

[60] A. Albrecht and N. Turok, *Evolution of Cosmic String Networks*, Phys. Rev. D **40** (1989) 973.

[61] B. Allen and E. P. S. Shellard, *Cosmic string evolution: a numerical simulation*, Phys. Rev. Lett. **64** (1990) 119.

[62] C. J. A. P. Martins and E. P. S. Shellard, *Extending the velocity dependent one scale string evolution model*, Phys. Rev. D **65** (2002) 043514 [hep-ph/0003298].

[63] C. Ringeval, M. Sakellariadou and F. Bouchet, *Cosmological Evolution of Cosmic String Loops*, JCAP **02** (2007) 023 [astro-ph/0511646].

[64] V. Vanchurin, K. D. Olum and A. Vilenkin, *Scaling of Cosmic String Loops*, Phys. Rev. D **74** (2006) 063527 [gr-qc/0511159].

[65] C. J. A. P. Martins and E. P. S. Shellard, *Fractal Properties and Small-Scale Structure of Cosmic String Networks*, Phys. Rev. D **73** (2006) 043515 [astro-ph/0511792].

[66] K. D. Olum and V. Vanchurin, *Cosmic String Loops in the Expanding Universe*, Phys. Rev. D **75** (2007) 063521 [astro-ph/0610419].

[67] J. J. Blanco-Pillado, K. D. Olum and B. Shlaer, *Large Parallel Cosmic String Simulations: New Results on Loop Production*, Phys. Rev. D **83** (2011) 083514 [1101.5173].

[68] D. G. Figueroa, M. Hindmarsh and J. Urrestilla, *Exact Scale-Invariant Background of Gravitational Waves from Cosmic Defects*, Phys. Rev. Lett. **110** (2013) 101302 [1212.5458].

[69] C. J. A. P. Martins, I. Y. Rybak, A. Avgoustidis and E. P. S. Shellard, *Extending the velocity-dependent one-scale model for domain walls*, Phys. Rev. D **93** (2016) 043534 [1602.01322].

[70] Y. Gouttenoire, G. Servant and P. Simakachorn, *Kination Cosmology from Scalar Fields and Gravitational-Wave Signatures*, 2111.01150.

[71] M. Kawasaki, T. Sekiguchi, M. Yamaguchi and J. Yokoyama, *Long-Term Dynamics of Cosmological Axion Strings*, PTEP **2018** (2018) 091E01 [1806.05566].

[72] A. Vaquero, J. Redondo and J. Stadler, *Early Seeds of Axion Miniclusters*, JCAP **04** (2019) 012 [1809.09241].

[73] V. B. Klaer and G. D. Moore, *How to Simulate Global Cosmic Strings with Large String Tension*, JCAP **10** (2017) 043 [1707.05566].

[74] V. B. Klaer and G. D. Moore, *Global cosmic string networks as a function of tension*, JCAP **06** (2020) 021 [1912.08058].

[75] M. Hindmarsh, J. Lizarraga, A. Lopez-Eiguren and J. Urrestilla, *Scaling Density of Axion Strings*, Phys. Rev. Lett. **124** (2020) 021301 [1908.03522].

[76] D. G. Figueroa, M. Hindmarsh, J. Lizarraga and J. Urrestilla, *Irreducible background of gravitational waves from a cosmic defect network: update and*

comparison of numerical techniques, Phys. Rev. D **102** (2020) 103516 [2007.03337].

[77] M. Buschmann, J. W. Foster and B. R. Safdi, *Early-Universe Simulations of the Cosmological Axion*, Phys. Rev. Lett. **124** (2020) 161103 [1906.00967].

[78] M. Hindmarsh, J. Lizarraga, A. Lopez-Eiguren and J. Urrestilla, *Approach to scaling in axion string networks*, Phys. Rev. D **103** (2021) 103534 [2102.07723].

[79] T. Hiramatsu, M. Kawasaki, K. Saikawa and T. Sekiguchi, *Axion cosmology with long-lived domain walls*, JCAP **01** (2013) 001 [1207.3166].

[80] M. Dine, W. Fischler and M. Srednicki, *A Simple Solution to the Strong CP Problem with a Harmless Axion*, Phys. Lett. B **104** (1981) 199.

[81] A. R. Zhitnitsky, *On Possible Suppression of the Axion Hadron Interactions. (In Russian)*, *Sov. J. Nucl. Phys.* **31** (1980) 260.

[82] J. E. Kim, *Light Pseudoscalars, Particle Physics and Cosmology*, Phys. Rept. **150** (1987) 1.

[83] A. Vilenkin, *Gravitational Field of Vacuum Domain Walls and Strings*, Phys. Rev. D **23** (1981) 852.

[84] G. B. Gelmini, M. Gleiser and E. W. Kolb, *Cosmology of Biased Discrete Symmetry Breaking*, Phys. Rev. D **39** (1989) 1558.

[85] S. E. Larsson, S. Sarkar and P. L. White, *Evading the cosmological domain wall problem*, Phys. Rev. D **55** (1997) 5129 [hep-ph/9608319].

[86] G. Janssen et al., *Gravitational wave astronomy with the SKA*, PoS **AASKA14** (2015) 037 [1501.00127].

[87] L. Lentati et al., *European Pulsar Timing Array Limits On An Isotropic Stochastic Gravitational-Wave Background*, Mon. Not. Roy. Astron. Soc. **453** (2015) 2576 [1504.03692].

[88] G. Desvignes et al., *High-precision timing of 42 millisecond pulsars with the European Pulsar Timing Array*, Mon. Not. Roy. Astron. Soc. **458** (2016) 3341 [1602.08511].

[89] NANOGRAV collaboration, *The NANOGrav 11-year Data Set: Pulsar-timing Constraints On The Stochastic Gravitational-wave Background*, Astrophys. J. **859** (2018) 47 [1801.02617].

[90] A. Weltman et al., *Fundamental physics with the Square Kilometre Array*, Publ. Astron. Soc. Austral. **37** (2020) e002 [1810.02680].

[91] LISA collaboration, *Laser Interferometer Space Antenna*, 1702.00786.

[92] K. Yagi and N. Seto, *Detector configuration of DECIGO/BBO and identification of cosmological neutron-star binaries*, Phys. Rev. D **83** (2011) 044011 [1101.3940].

[93] AEDGE collaboration, *AEDGE: Atomic Experiment for Dark Matter and Gravity Exploration in Space*, EPJ Quant. Technol. **7** (2020) 6 [1908.00802].

[94] KAGRA, LIGO Scientific, Virgo, VIRGO collaboration, *Prospects for observing and localizing gravitational-wave transients with Advanced LIGO, Advanced Virgo and KAGRA*, Living Rev. Rel. **21** (2018) 3 [1304.0670].

[95] LIGO Scientific, VIRGO collaboration, *Characterization of the LIGO detectors during their sixth science run*, Class. Quant. Grav. **32** (2015) 115012 [1410.7764].

[96] LIGO Scientific, Virgo collaboration, *Search for the isotropic stochastic background using data from Advanced LIGO's second observing run*, Phys. Rev. D **100** (2019) 061101 [1903.02886].

[97] S. Hild et al., *Sensitivity Studies for Third-Generation Gravitational Wave Observatories*, Class. Quant. Grav. **28** (2011) 094013 [1012.0908].

[98] M. Punturo et al., *The Einstein Telescope: A third-generation gravitational wave observatory*, Class. Quant. Grav. **27** (2010) 194002.

[99] LIGO Scientific collaboration, *Exploring the Sensitivity of Next Generation Gravitational Wave Detectors*, Class. Quant. Grav. **34** (2017) 044001 [1607.08697].

[100] M. Breitbach, J. Kopp, E. Madge, T. Opferkuch and P. Schwaller, *Dark, Cold, and Noisy: Constraining Secluded Hidden Sectors with Gravitational Waves*, JCAP **07** (2019) 007 [1811.11175].

[101] A. Vilenkin and A. E. Everett, *Cosmic Strings and Domain Walls in Models with Goldstone and PseudoGoldstone Bosons*, Phys. Rev. Lett. **48** (1982) 1867.

[102] C. J. A. P. Martins and E. P. S. Shellard, *Quantitative string evolution*, Phys. Rev. D **54** (1996) 2535 [hep-ph/9602271].

[103] L. Sousa and P. P. Avelino, *Stochastic Gravitational Wave Background generated by Cosmic String Networks: Velocity-Dependent One-Scale model versus Scale-Invariant Evolution*, Phys. Rev. D **88** (2013) 023516 [1304.2445].

[104] L. Sousa and P. P. Avelino, *Stochastic gravitational wave background generated by cosmic string networks: The small-loop regime*, Phys. Rev. D **89** (2014) 083503 [1403.2621].

[105] J. R. C. C. C. Correia and C. J. A. P. Martins, *Extending and Calibrating the Velocity dependent One-Scale model for Cosmic Strings with One Thousand Field Theory Simulations*, Phys. Rev. D **100** (2019) 103517 [1911.03163].

[106] T. Hiramatsu, M. Kawasaki and K. Saikawa, *Evolution of String-Wall Networks and Axionic Domain Wall Problem*, JCAP **08** (2011) 030 [1012.4558].

[107] J. Preskill, S. P. Trivedi, F. Wilczek and M. B. Wise, *Cosmology and broken discrete symmetry*, Nucl. Phys. B **363** (1991) 207.

[108] M. Gleiser and R. Roberts, *Gravitational waves from collapsing vacuum domains*, Phys. Rev. Lett. **81** (1998) 5497 [astro-ph/9807260].

[109] T. Hiramatsu, M. Kawasaki and K. Saikawa, *Gravitational Waves from Collapsing Domain Walls*, JCAP **05** (2010) 032 [1002.1555].

[110] M. Kawasaki and K. Saikawa, *Study of gravitational radiation from cosmic domain walls*, JCAP **09** (2011) 008 [1102.5628].

[111] T. Hiramatsu, M. Kawasaki and K. Saikawa, *On the estimation of gravitational wave spectrum from cosmic domain walls*, JCAP **02** (2014) 031 [1309.5001].

[112] R. Zambujal Ferreira, A. Notari, O. Pujolàs and F. Rompineve, *High Quality QCD Axion at Gravitational Wave Observatories*, Phys. Rev. Lett. **128** (2022) 141101 [2107.07542].

[113] K. Saikawa, *Gravitational waves from cosmic domain walls: a mini-review*, J. Phys. Conf. Ser. **1586** (2020) 012039.

[114] C. O'Hare, "cajohare/axionlimits: Axionlimits."

https://cajohare.github.io/AxionLimits/, July, 2020. 10.5281/zenodo.3932430.

[115] A. Mitridate and D. Wright, *Ptarcade - data*, .

[116] J. A. Ellis, M. Vallisneri, S. R. Taylor and P. T. Baker, "Enterprise: Enhanced numerical toolbox enabling a robust pulsar inference suite." Zenodo, Sept., 2020. 10.5281/zenodo.4059815.

[117] S. R. Taylor, P. T. Baker, J. S. Hazboun, J. Simon and S. J. Vigeland, *enterprise_extensions*, 2021.

[118] H. Jeffreys, *The theory of probability*. OuP Oxford, 1998.

[119] Planck collaboration, *Planck 2018 results. VI. Cosmological parameters*, Astron. Astrophys. **641** (2020) A6 [1807.06209].

[120] P. Simakachorn, *Charting Cosmological History and New Particle Physics with Primordial Gravitational Waves*, Ph.D. thesis, Hamburg U., 10, 2022.

[121] A. Ghoshal, Y. Gouttenoire, L. Heurtier and P. Simakachorn, *Primordial Black Hole Archaeology with Gravitational Waves from Cosmic Strings*, 2304.04793.

[122] Y. Bai, T.-K. Chen and M. Korwar, *QCD-Collapsed Domain Walls: QCD Phase Transition and Gravitational Wave Spectroscopy*, 2306.17160.

[123] M. Bauer, M. Heiles, M. Neubert and A. Thamm, *Axion-Like Particles at Future Colliders*, Eur. Phys. J. C **79** (2019) 74 [1808.10323].

[124] A. Hook, S. Kumar, Z. Liu and R. Sundrum, *High Quality QCD Axion and the LHC*, Phys. Rev. Lett. **124** (2020) 221801 [1911.12364].

[125] M. Bauer, M. Neubert, S. Renner, M. Schnubel and A. Thamm, *Flavor probes of axion-like particles*, JHEP **09** (2022) 056 [2110.10698].

[126] G. Alonso-Álvarez, J. Jaeckel and D. D. Lopes, *Tracking axion-like particles at the LHC*, 2302.12262.

[127] D. Cadamuro and J. Redondo, *Cosmological bounds on pseudo Nambu-Goldstone bosons*, JCAP **02** (2012) 032 [1110.2895].

[128] P. F. Depta, M. Hufnagel and K. Schmidt-Hoberg, *Robust cosmological constraints on axion-like particles*, JCAP **05** (2020) 009 [2002.08370].

[129] A. Hook, G. Marques-Tavares and D. Racco, *Causal gravitational waves as a probe of free streaming particles and the expansion of the Universe*, JHEP **02** (2021) 117 [2010.03568].

[130] D. Racco and D. Poletti, *Precision cosmology with primordial GW backgrounds in presence of astrophysical foregrounds*, JCAP **04** (2023) 054 [2212.06602].

[131] G. Franciolini, D. Racco and F. Rompineve, *Footprints of the QCD Crossover on Cosmological Gravitational Waves at Pulsar Timing Arrays*, 2306.17136.

[132] S. Blasi, A. Mariotti, A. Rase and A. Sevrin, *Axionic domain walls at Pulsar Timing Arrays: QCD bias and particle friction*, 2306.17830.

[133] T. Vachaspati, *Lunar Mass Black Holes from QCD Axion Cosmology*, 1706.03868.

[134] F. Ferrer, E. Masso, G. Panico, O. Pujolas and F. Rompineve, *Primordial Black Holes from the QCD axion*, Phys. Rev. Lett. **122** (2019) 101301 [1807.01707].

[135] Y. Gouttenoire and E. Vitagliano, *Domain wall interpretation of the PTA signal confronting black hole overproduction*, 2306.17841.

[136] N. Kitajima, J. Lee, K. Murai, F. Takahashi and W. Yin, *Nanohertz Gravitational Waves from Axion Domain Walls Coupled to QCD*, 2306.17146.

[137] B.-Q. Lu and C.-W. Chiang, *Nano-Hertz stochastic gravitational wave background from domain wall annihilation*, 2307.00746.

[138] C. J. A. P. Martins, I. Y. Rybak, A. Avgoustidis and E. P. S. Shellard, *Stretching and Kibble scaling regimes for Hubble-damped defect networks*, Phys. Rev. D **94** (2016) 116017 [1612.08863].

[139] A. Friedland, H. Murayama and M. Perelstein, *Domain walls as dark energy*, Phys. Rev. D **67** (2003) 043519 [astro-ph/0205520].

[140] G. S. F. Guedes, P. P. Avelino and L. Sousa, *Signature of inflation in the stochastic gravitational wave background generated by cosmic string networks*, Phys. Rev. D **98** (2018) 123505 [1809.10802].

[141] Y. Cui, M. Lewicki and D. E. Morrissey, *Gravitational Wave Bursts as Harbingers of Cosmic Strings Diluted by Inflation*, Phys. Rev. Lett. **125** (2020) 211302 [1912.08832].

[142] L. Liu, Z.-C. Chen and Q.-G. Huang, *Implications for the non-Gaussianity of curvature perturbation from pulsar timing arrays*, 2307.01102.

[143] D. G. Figueroa, M. Pieroni, A. Ricciardone and P. Simakachorn, *Cosmological Background Interpretation of Pulsar Timing Array Data*, 2307.02399.

[144] C. Caprini and D. G. Figueroa, *Cosmological Backgrounds of Gravitational Waves*, Class. Quant. Grav. **35** (2018) 163001 [1801.04268].

[145] K. Saikawa and S. Shirai, *Primordial gravitational waves, precisely: The role of thermodynamics in the Standard Model*, JCAP **05** (2018) 035 [1803.01038].

Supplemental Material

This *supplemental material* gives more details on the analysis of NG15 data with the global-strings and domain-wall templates. App. A specifies the priors used in the analysis. We then present in App. B the best-fits without and with the astrophysical background and compare them using the Bayes Factor (BF) method. App. C presents the results of global string template in the limit $T_{\rm dec} \to 0$ (or $m_a \to 0$), the so-called *stable* global strings. Our analysis includes the temperature dependence of the number of relativistic degrees of freedom g_* and g_{*s}, taken from Ref. [145].

Appendix A: Priors for Analysis

Tab. I shows the ranges of priors for the parameters in global-string and domain-wall scenarios, used for the Monte Carlo Markov Chain tools. For the SMBHB signal, we use the prior of power-law fitted spectrum, which is translated from the 2D Gaussian distribution in SMBHB parameters, motivated by the simulated SMBHB populations [7] and implemented in `PTArcade`. The Bayes factors reported for our two new-physics cases depend on the evidence of this SMBHB template.

Models	Parameters	Priors
Global strings	f_a [GeV]: $U(1)$ breaking scale	log–uniform:$[10^{15}, 10^{17}]$
	$T_{\rm dec}$ [GeV] : Temperature when string network decays	log–uniform:$[10^{-8}, 10]$
	(related to axion mass m_a via Eq. (3))	
Domain walls	$\alpha_\star$: Energy fraction in DWs at decay	log–uniform:$[10^{-2}, 1]$
	$T_\star$ [GeV] : DW annihilation temperature	log–uniform:$[10^{-3}, 10]$
	δ : Width of GW spectrum	uniform:$[1, 3]$
	β : Slope of GW spectrum for $f > f_{\rm p}$	uniform:$[1, 3]$

TABLE I. Ranges of priors for global-string and domain-wall parameters used for the analysis.

Appendix B: Global-String and Domain-Wall signals without SMBHB background

In contrast with the analysis presented in the main text which interprets the NG15 signal in terms of SMBHBs, in this appendix we assume the absence of astrophysical background and instead interpret the signal as a SGWB from global strings or domain walls. Fig. 5 shows the 2-dimensional posterior of the global-string and the domain-wall parameters. For global strings, the best-fit (max. posterior) is at $f_a = 9.55^{+2.19}_{-1.63} \cdot 10^{15}$ GeV and $T_{\rm dec} = 3.16^{+1.88}_{-1.15}$ MeV at 68% CL. The central value of $T_{\rm dec}$ correspond to $m_a = 3.89 \cdot 10^{-15}$ eV; *cf.* Eq. (3). For domain walls, the best-fit is at $\alpha_\star = 0.111^{+0.045}_{-0.027}$ and $T_\star = 125^{+31}_{-39}$ MeV, with the error within the 68% CL region. Their central values give $m_a F_a^2 = 2.4 \cdot 10^{15}$ GeV^3; *cf.* Eq. (6). We calculate the Bayes Factor (compared to the SGWB from SMBHBs) from `PTArcade` and find that the BFs are 22.8 for global strings and 23.4 for domain walls. When the SMBHB background is added, we find that the BF for both cases increases to 26.0 for global strings and 44.7 for domain walls. However, the values of the best-fitted parameters change only slightly: $f_a = 9.87^{+2.67}_{-2.02} \cdot 10^{15}$ GeV and $T_{\rm dec} = 3.50^{+2.44}_{-1.48}$ MeV, at 68% CL for global strings, corresponding to $m_a = 4.78 \cdot 10^{-15}$ eV. For domain walls, we have $\alpha_\star = 0.114^{+0.060}_{-0.033}$ and $T_\star = 128^{+55}_{-33}$ MeV, corresponding to $m_a F_a^2 = 2.6 \cdot 10^{15}$ GeV^3.

Appendix C: Global strings for $m_a \to 0$

The constrained region in Fig. 2-middle shows that the PTA signal from global strings with small $T_{\rm dec}$ (or small m_a) reaches the asymptotic value of $f_a \simeq 2.8 \cdot 10^{15}$ GeV. This is because the cut-off specified by $T_{\rm dec}$ moves outside of the PTA range and the SGWB spectrum is seen as the one from stable global strings in the limit $T_{\rm dec}$ or $m_a \to 0$. Fig. 6-left shows the 1D posterior of signal from the stable global strings, which has the best-fitted spectrum at $f_a \simeq 2.99^{+0.31}_{-0.26} \times 10^{15}$ GeV at 68% CL. Nonetheless, it has the BF of 1.45×10^{-3} due to its red-tilted spectrum, poorly fitting the data, as shown in Fig. 6-middle. When the SMBHB background is added in Fig. 6-right, the BF becomes 0.64, meaning that the stable string spectrum worsens the fit compared to the SMBHB alone. Although the fit is not good, the constraint can be derived when the global-string SGWB becomes too strong (too large f_a) using the

K-ratio, discussed in the main text. The vertical solid line in Fig. 6-right shows the limit set by the NG15 data (K-ratio $= 0.1$): $f_a < 2.77 \cdot 10^{15}$ GeV, which is similar to bound obtain from Fig. 2-middle in the $T_{\rm dec} \to 0$ limit.

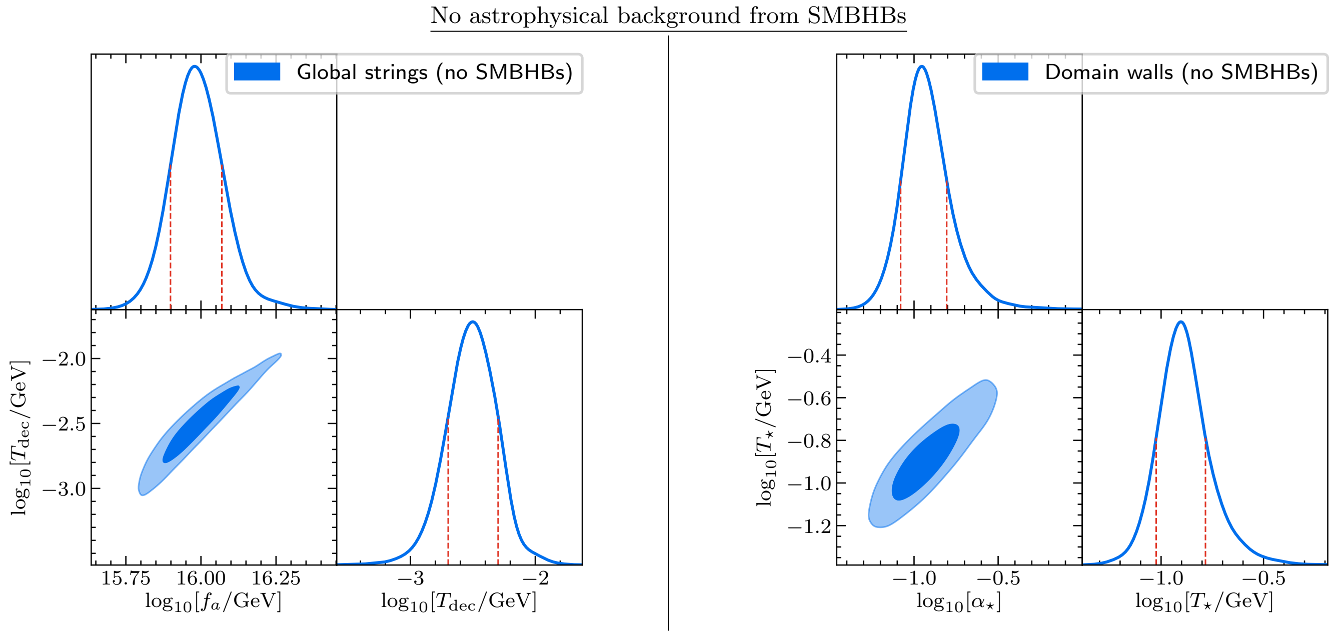

FIG. 5. Best fits to NG15 data. *Left:* The 2D posterior for the global-string SGWB template presented in the main text. Via Eq. (3), the best-fit corresponds to axion parameters $\{f_a, m_a\} = \{9.55 \cdot 10^{15}\ \text{GeV}, 3.89 \cdot 10^{-15}\ \text{eV}\}$. The comparison of the fit to the SMBHB signal yields the BF $\simeq 22.8$. *Right:* Result for domain-wall SGWB, which has the BF $\simeq 23.4$. The best-fitted axion parameters satisfy $m_a F_a^2 = 2.4 \cdot 10^{15}$ GeV^3; *cf.* Eq. (6). The posteriors for the UV slope β and the width δ are not constrained as only the IR tail of the spectrum (9) lies within the PTA frequency range for the chosen range of T_*.

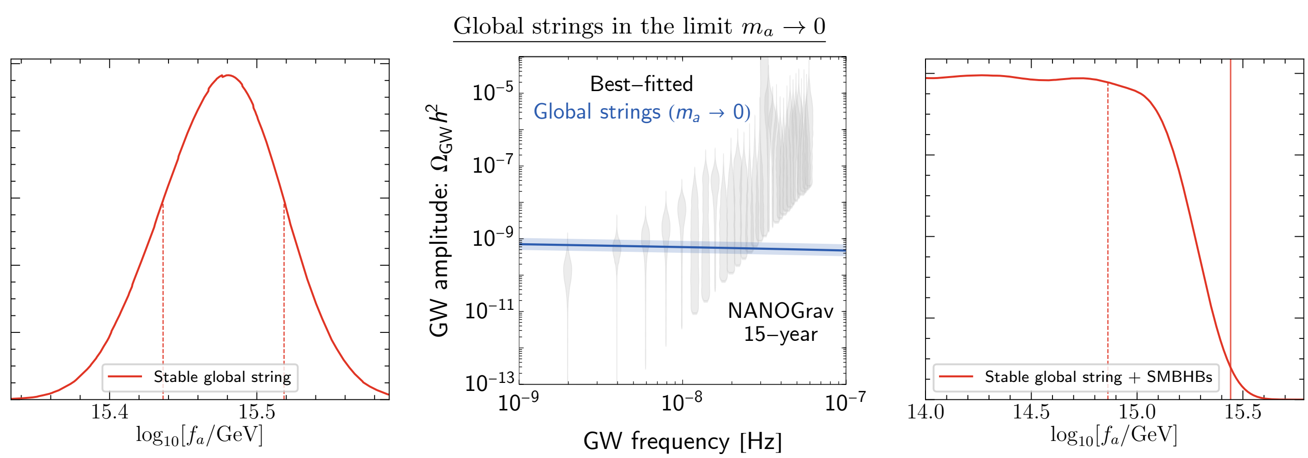

FIG. 6. *Left:* The 1D posterior of the stable global-string SGWB, using NG15 data set. The best-fitted f_a value is $f_a \simeq 2.99^{+0.31}_{-0.26} \times 10^{15}$ GeV at 68% CL and the BF is 1.45×10^{-3}, for the comparison with the SMBHBs. The vertical red line indicates the 1-σ region. *Middle:* The best-fitted GW background from stable global strings and its range within 1σ region of f_a, laying over the violins of NG15 observation. *Right:* The 1D posterior of the stable global-string SGWB + SMBHBs contribution, fitted to NG15 data set. The best-fitted string scale is $f_a \simeq 1.83^{+5.45} \times 10^{15}$ GeV at 68% CL and the BF of 0.64, compared to the SMBHBs alone. The vertical dashed line locates the 1σ region, while the solid vertical line marks the K-ratio $= 0.1$ and sets a limit on $f_a < 2.77 \times 10^{15}$ GeV.